Focus Section: February 2023 SE Türkiye Earthquakes

The Role of Stress Transfer in Rupture Nucleation and Inhibition in the 2023 Kahramanmaraş, Türkiye, Sequence, and a One-Year Earthquake Forecast

Shinji Toda[*1] and Ross S. Stein[2]

Abstract

We probe the interaction of large earthquakes on the East Anatolian fault zone, site of four $M_w \geq 6.8$ events since 2020. We find that the 2023 M_w 7.8 Pazarcık shock promoted the M_w 7.7 Elbistan earthquake 9 hr later, largely through unclamping of the epicentral patch of the future rupture. Epicentral unclamping is also documented in the 1987 Superstition Hills, 1997 Kagoshima, and 2019 Ridgecrest sequences, so this may be common. The M_w 7.7 Elbistan earthquake, in turn, is calculated to have reduced the shear stress on the central Pazarcık rupture, producing a decrease in the aftershock rate along that section of the rupture. Nevertheless, the M_w 7.7 event ruptured through a Çardak fault section on which the shear stress was decreased by the M_w 7.8 rupture, and so rupture propagation was not halted by the static stress decrease. The 2020 M_w 6.8 Doğanyol–Sivrice earthquake, located beyond the northeast tip of the M_w 7.8 Pazarcık rupture, locally dropped the stress by ~ 10 bars. The 2023 M_w 7.8 earthquake then increased the stress there by 1–2 bar, leaving a net stress drop, resulting in a hole in the 2023 Pazarcık aftershocks. We find that many lobes of calculated stress increase caused by the 2020–2023 M_w 6.8–7.8 earthquakes are sites of aftershocks, and we calculate 5–10 faults in several locations off the ruptures brought closer to failure. The earthquakes also cast broad stress shadows in which most faults were brought farther from failure, and we observe the beginnings of seismicity rate decreases in some of the deepest stress shadows. Some 41 $M_w \geq 5$ aftershocks have struck since the M_w 7.8 mainshock. But based on these Coulomb interactions and on the rapid Kahramanmaraş aftershock decay, we forecast only about 1–3 $M_w \geq 5$ earthquakes during the 12–month period beginning 1 December 2023, which is fortunately quite low.

Cite this article as Toda, S., and R. S. Stein (2024). The Role of Stress Transfer in Rupture Nucleation and Inhibition in the 2023 Kahramanmaraş, Türkiye, Sequence, and a One-Year Earthquake Forecast, *Seismol. Res. Lett.* **XX**, 1–11, doi: 10.1785/0220230252.

Supplemental Material

Introduction

The 2023 Kahramanmaraş earthquakes took the lives of 53,000 people, left 2 million homeless, collapsed 30,000 buildings, and is expected to cost about $34 billion (Çetin *et al.*, 2023; Erdik *et al.*, 2023). Among the many tragic and alarming elements of the earthquakes in Türkiye are some that can occur worldwide. These include the possibility of great events on secondary faults (Hussain *et al.*, 2023; Karabacak *et al.*, 2023), and interacting mainshocks that attack buildings twice. For example, in Malatya, close to both ruptures, some buildings weakened in the first quake collapsed in the second. Here, we focus on earthquake interaction to probe the triggering mechanism, to assess where the hazard has changed on surrounding faults, and to furnish a testable 1-year earthquake forecast.

There is some ambiguity among the reporting agencies about the Kahramanmaraş sequence names and magnitudes. Here, we adopt the Disaster and Emergency Management Authority of Türkiye (AFAD) naming convention, Global Centroid Moment Tensor (Global CMT) magnitudes and seismic moments, and use the U.S. Geological Survey (USGS) finite-fault models (Table 1). Perhaps most important, the two shocks are similar in size, and so can be considered a double event.

Stress Transferred by the M_w 7.8 Pazarcık Earthquake to the Sürgü–Cardak Fault

A fundamental question of this sequence is whether the M_w 7.8 Pazarcık rupture promoted or triggered the M_w 7.7 Elbistan

1. International Research Institute of Disaster Science (IRIDeS), Tohoku University, Sendai, Japan, https://orcid.org/0000-0002-3913-5303 (ST); 2. Temblor, Inc., Tiburon, California, U.S.A., https://orcid.org/0000-0002-0029-4964 (RSS)

*Corresponding author: toda@irides.tohoku.ac.jp

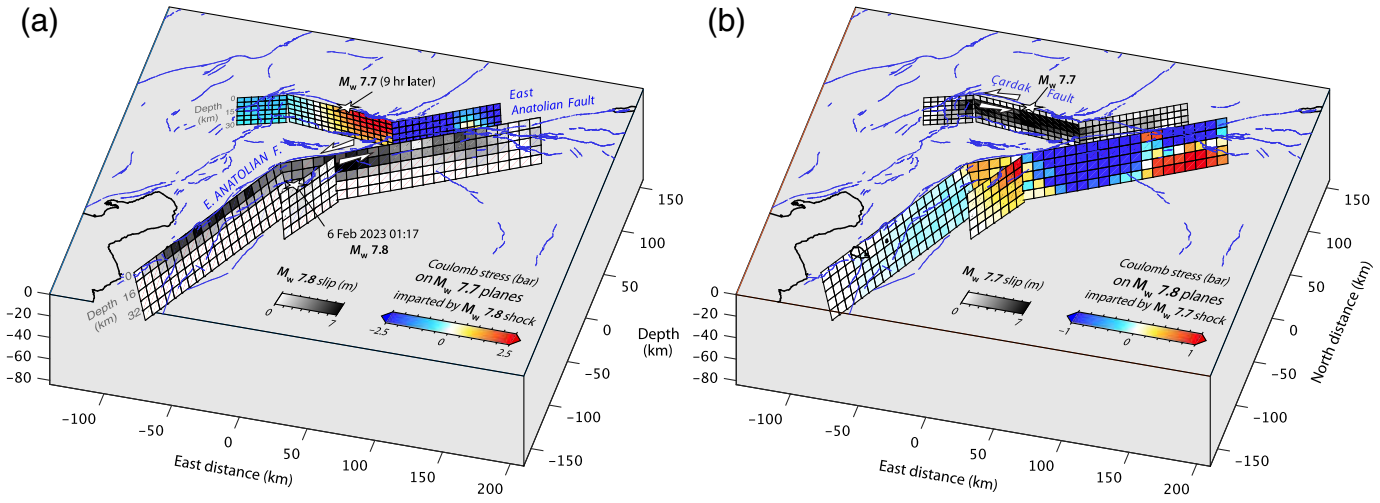

Figure 1. Stress interaction of the 6 February 2023 M_w 7.8 and 7.7 earthquake ruptures. (a) The first event brought the epicentral patch of the Çardak fault about 3 bars closer to Coulomb failure, but inhibited failure on the eastern ruptured section of the fault. (b) The M_w 7.7 event then brought a central portion of the M_w 7.8 rupture farther from failure, suggesting that rupture nucleation is more influenced by the static stress changes than is propagation. Note that the scale bar is saturated at ±1 bar. The color version of this figure is available only in the electronic edition.

shock, which struck 9 hr later, 100 km to the north on a separate fault, and if so, how. Using the version 3 (17 February 2023) USGS source models (Goldberg *et al.*, 2023; Figs. S1 and S2, available in the supplemental material to this article), we find that the M_w 7.8 earthquake increased the calculated Coulomb stress by 1–4 bars along the epicentral section of the Çardak fault (Fig. 1a), as previously reported by Toda *et al.* (2023) and subsequently by Jia *et al.* (2023), Melgar *et al.* (2023), and U.S. Geological Survey (USGS) Geologic Hazards Science Center and Collaborators (2023). In this and all subsequent calculations, we use a 0.4 coefficient of friction on receiver faults (faults receiving stress). This is certainly a simplification, as friction could be anywhere from 0.0–0.8, but one that is widely used in Coulomb stress transfer analyses. Parsons (2005), for example, finds that friction uncertainty leads to a 20%–50% variation in the calculated stress change.

The M_w 7.8 rupture on the East Anatolian fault also decreased the Coulomb stress by 3–10 bars along the section of the Çardak fault that is aligned parallel to the East Anatolian fault (Fig. 1a). But the M_w 7.7 rupture nevertheless propagated through this inhibited section. In Melgar *et al.* (2023), the rupture front does not appear to pause or slow down as it enters the inhibited section of the Çardak fault, suggesting that once a rupture propagates, the large dynamic (transient) tip stresses dominate over the much smaller static stress changes.

We can further resolve the Coulomb stress components on the Çardak fault. Although the left-lateral shear stress on the M 7.7 epicentral patch was increased by ∼1 bar (Fig. 2a), it was unclamped by a much larger 3–5 bars (Fig. 2b). Unclamping at the site of a large subsequent shock has been documented for at least three other earthquake pairs: 1987 Superstition Hills sequence (Hudnut *et al.*, 1989), the 1988–1989 Lake Elsman–Loma Prieta earthquakes (Perfettini *et al.*, 1999), and secondary oblique-slip faults surrounding the 1989 Loma Prieta earthquake (Parsons *et al.*, 1999). But perhaps the strongest example of fault unclamping is the M_w 6.4 and 7.1 Ridgecrest earthquakes that struck 31 hr apart on orthogonal surfaces (Toda and Stein, 2020), in which both the shear stress and unclamping increased on the M_w 7.1 epicentral patch (Fig. 3b); and the 1997 Kagoshima doublet

TABLE 1
2023 Kahramanmaraş Mainshock Magnitudes and Seismic Moments

	Pazarcık Earthquake		Elbistan Earthquake		Pazarcık/Elbistan
Source	**M_w**	**M_0 (N·m)**	**M_w**	**M_w (N·m)**	**M_0 Ratio**
Global CMT	7.8	5.8×10^{20}	7.7	4.5×10^{20}	1.3
USGS	7.8	5.4×10^{20}	7.5	2.6×10^{20}	2.1
USGS FF*	7.9	7.9×10^{20}	7.8	5.0×10^{20}	1.6
AFAD	7.7		7.6		

*U.S. Geological Survey (USGS) finite-fault (FF) model (Goldberg *et al.*, 2023). AFAD, Disaster and Emergency Management Authority of Türkiye; Global CMT, Global Centroid Moment Tensor.

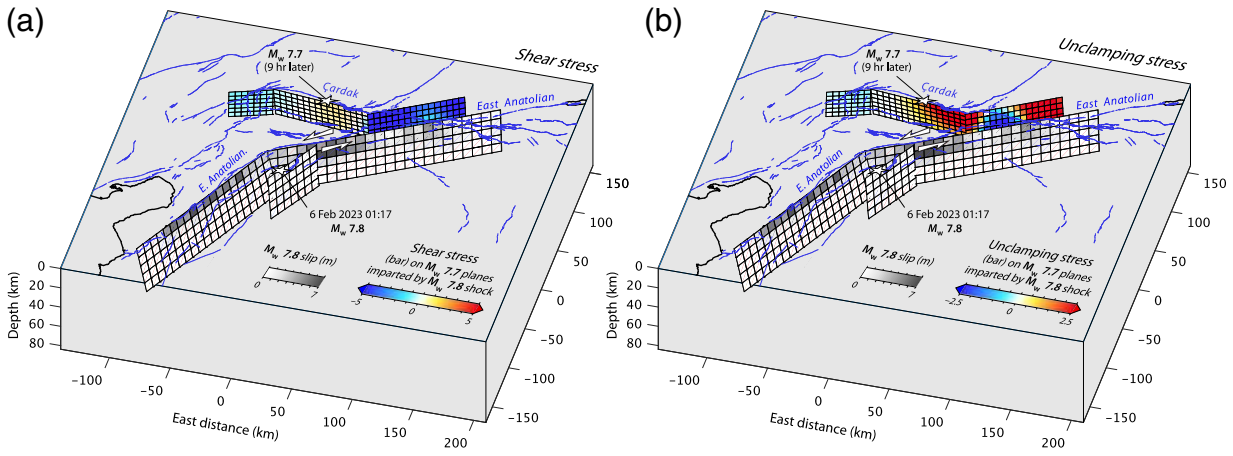

Figure 2. Stress components imparted by the M_w 7.8 shock on the Çardak fault. (a) The shear stress increase is about 1 bar, whereas (b) the unclamping stress is a much larger 3–5 bar. Note that the scale bar saturation is different in panels (a) and (b). The color version of this figure is available only in the electronic edition.

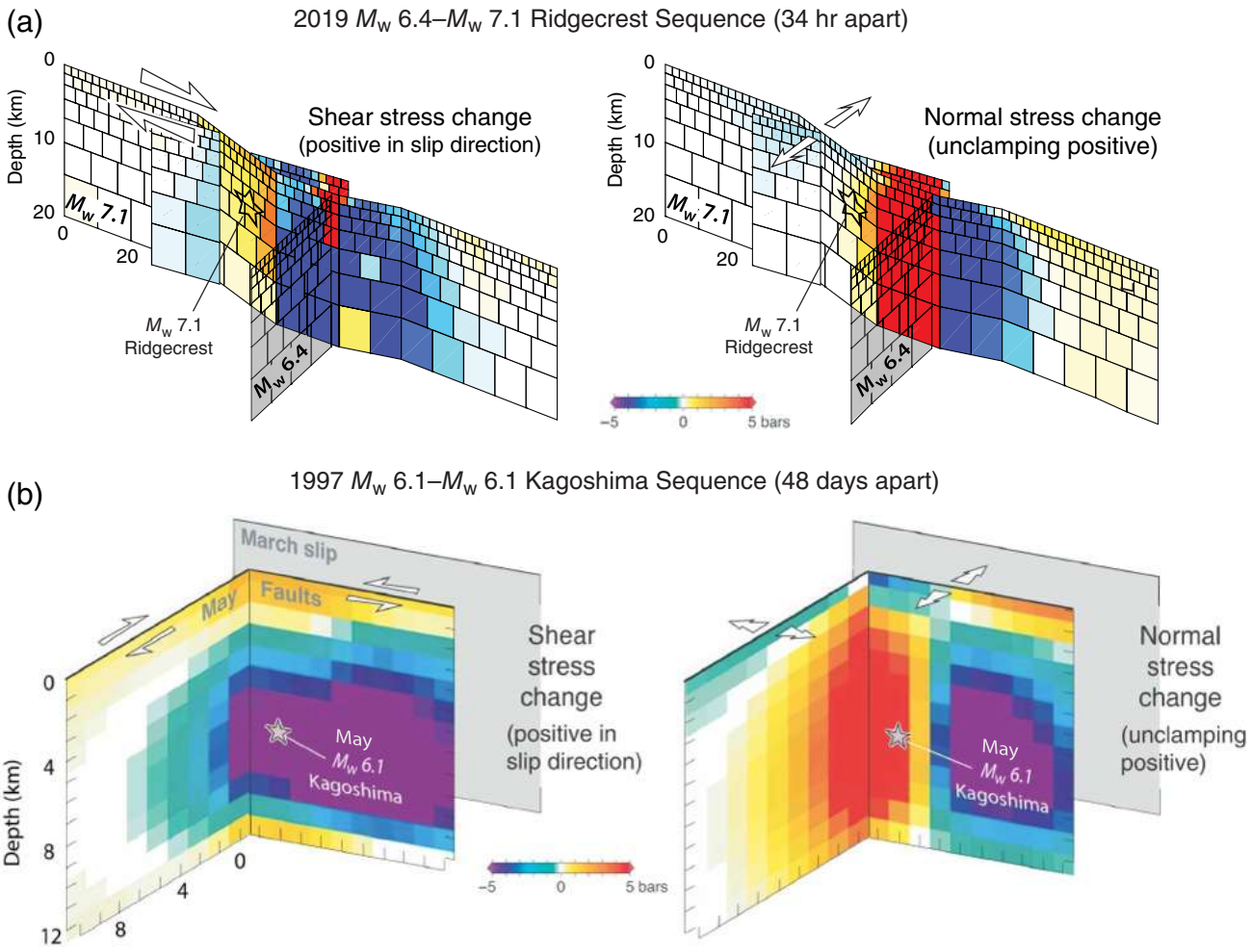

Figure 3. Two cases resembling Kahramanmaraş, in which the second fault was unclamped by the first rupture. (a) The 2019 Ridgecrest sequence, in which the M_w 6.4 event struck on the translucent orthogonal surface. This Ridgecrest calculation is not shown in Toda and Stein (2020), and we note that Barnhart *et al.* (2019) reached a different conclusion about the stress components. (b) The 1997 Kagoshima doublet (Toda and Stein, 2003). The color version of this figure is available only in the electronic edition.

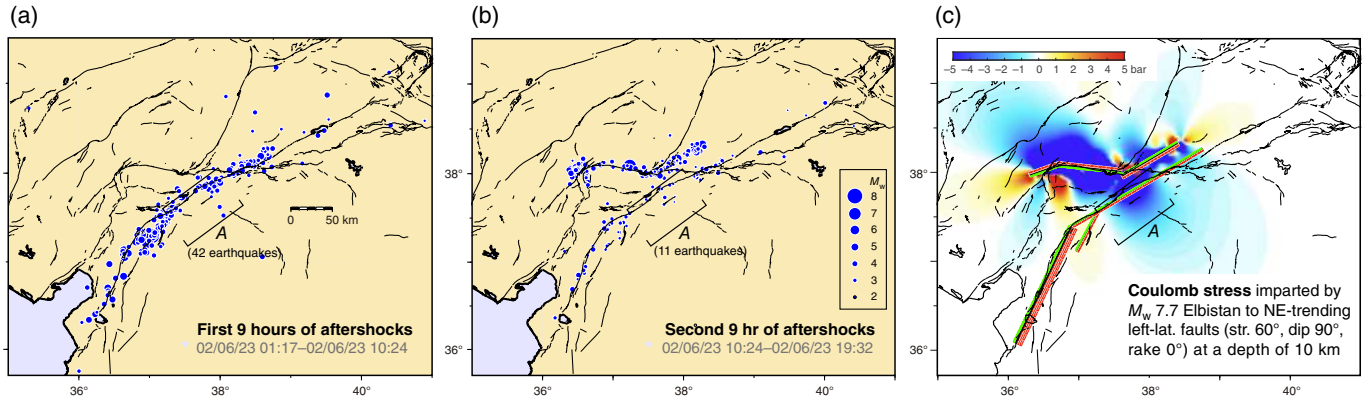

(Fig. 3b), mainshocks for which struck 4 months apart (Toda and Stein, 2003).

Whether unclamping (reduced normal stress) or a Coulomb stress increase is more important in promoting failure is under debate. Parsons *et al.* (1999) argued that for limited-offset oblique faults, unclamping dominates, whereas for major strike-slip faults, the Coulomb stress is best correlated with triggering. With a slip rate of 2.5 mm/yr (Duman and Emre, 2013), the Çardak fault likely has a more limited left-lateral offset than the longer and more rapidly slipping East Anatolian fault (10 mm/yr). The other examples shown in Figure 3 also likely have small cumulative displacement, and so the Parsons *et al.* (1999) inference may be correct.

Stress Transferred by the M_w 7.7 Elbistan Earthquake to the East Anatolian Fault

The aftershock rate along the central 60 km of the M_w 7.8 rupture appears to have dropped at the time of the M_w 7.7 shock (compare Fig. 4a,b). We calculate that the M_w 7.7 shock draped a stress shadow across this section of the M_w 7.8 rupture (resolved on the fault plane in Fig. 1b and in map view in Fig. 4c). This shadow occurs because the northwestern sections of the M_w 7.8 and 7.7 ruptures are parallel to each other and only 25 km apart, and so the stress drop centered along the Çardak fault extends to the East Anatolian fault.

Impact of the 2020–2023 M_w 6.8–7.8 Earthquakes on the Surrounding Faults

In addition to roughly 25-km-wide zones of aftershocks along the M_w 7.8 and M_w 7.7 ruptures, there are seismicity rate increases beyond all four rupture tips, and near several fault bends (Fig. 5a). Most of these increases correspond to calculated Coulomb stress increases (Fig. 5b). It typically takes several years to measure seismicity rate decreases, but in the 143-day postmainshock observation period, two regions in which the seismicity rate dropped by a factor of 3 or more over the background rate have emerged (dotted polygons in Fig. 5a); these lie in the calculated stress shadows.

Figure 4. Change in aftershock distribution after the second (M_w 7.7) earthquake strikes. (a) Initially, aftershock density is fairly uniform along the 300-km-long East Anatolian fault rupture. (b) After the M_w 7.7 shock strikes, the central portion (site *A*) is less productive. (c) The diminished aftershock rate roughly coincides with the calculated stress shadow cast by the Elbistan M_w 7.7 shock. Although completeness could be different in the two time periods, the aftershocks have similar *b*-values (Fig. S3c,d), and so are likely comparable. Stresses are resolved on the M_w 7.8 rupture plane in Figure 1b. The color version of this figure is available only in the electronic edition.

The sites of calculated Coulomb stress increase also correspond to stress increases on focal mechanisms, with focal mechanisms beyond the fault tips generally yellow (0.05 bar; Fig. 6). As a control, we find the percentage of the background mechanisms promoted by the 2023 M_w 7.8 and 7.7 shocks, which of course had not occurred (Fig. 6a), which can be compared with the percentage of promoted aftershock mechanisms (Fig. 6b and inset histogram). The increase from 55% to 62% is a measure of the extent to which the calculated stress change can explain the aftershock distribution, in which an increase from 50% to 100% would be a perfect fit. Another test of the stress calculation is the mean stress change on focal mechanisms (within a ±10 bar range). For the background it is −0.18 bar; for the aftershocks it is +0.65 bar, an increase of 0.83 bar.

Interaction of the 2020 M_w 6.8 Doğanyol–Sivrice and 2023 M_w 7.8 Pazarcık Earthquakes

The 2020 M_w 6.8 earthquake (Cheloni and Akinci, 2020), which did not rupture to the surface, is located 50–75 km from the northeast tip of the 2023 M_w 7.8 Pazarcık rupture. Aftershocks (Fig. 7a) in the high-slip zone of the 2020 earthquake decayed rapidly to the background rate (Fig. 7b) in 2–3 yr (the central white–yellow zone in Fig. 7c), and so the aftershock sequence appeared to have ended before the 2023 M_w 7.8 earthquake struck. In contrast, beyond the M_w 6.8 rupture tips, we project the M_w 6.8 aftershock sequence will persist for more than

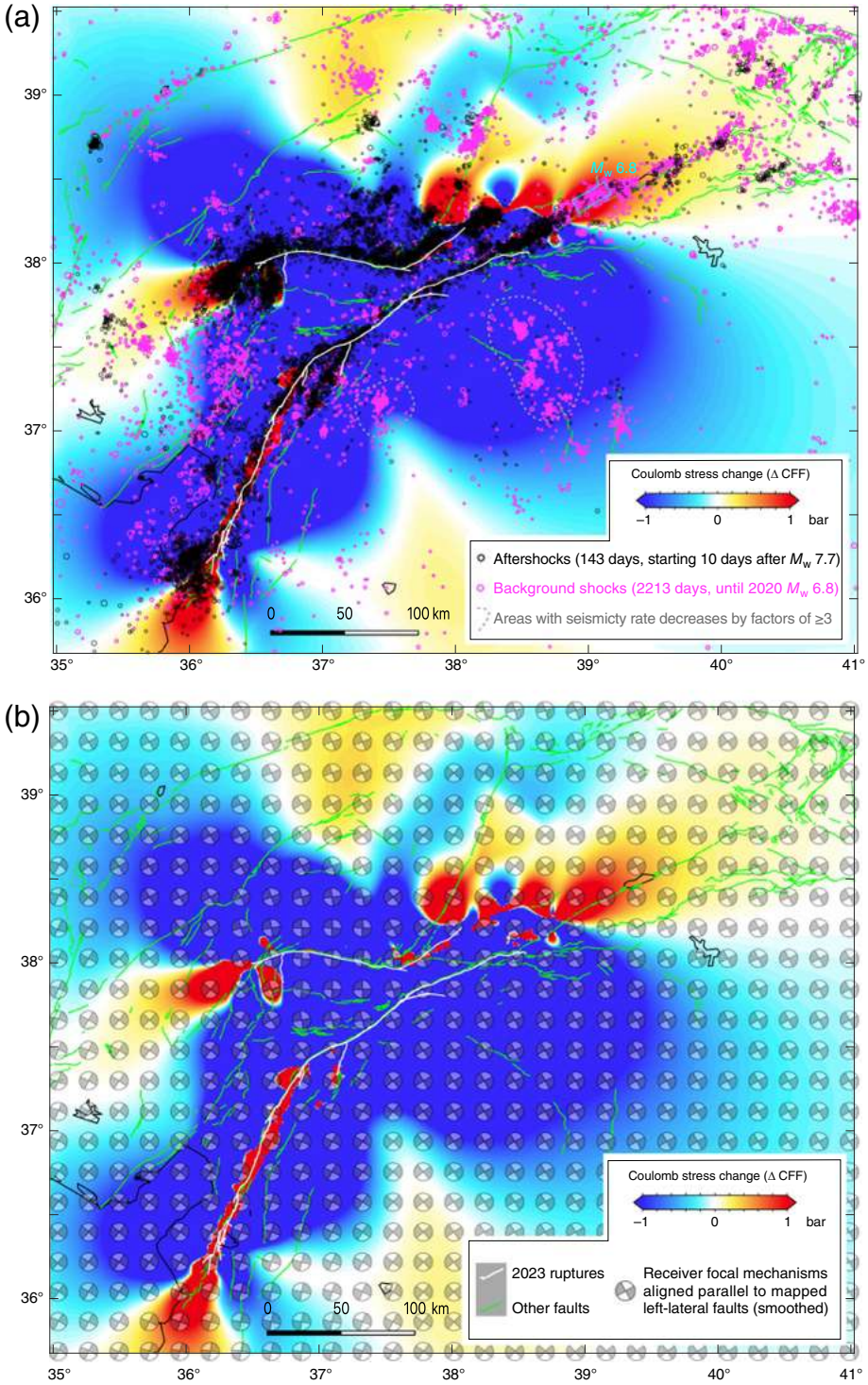

Figure 5. Coulomb stress imparted to smoothed, simplified surrounding "receiver" faults (faults that receive stress from the 2023 M_w 7.8 and 7.7 mainshocks), with $M_w \geq 2$ Disaster and Emergency Management Authority of Türkiye (AFAD) background seismicity and aftershocks. (a) In addition to the large, blue "stress shadow", where aftershocks are rare, there are concentrated red "stress trigger zones" along portions of the ruptures and beyond their tips, many of which are associated with aftershocks. (b) Here, we use left-lateral focal mechanisms conforming to faults (green lines) mapped by Emre *et al.* (2018), ignoring normal mechanisms. The white lines are surface ruptures of the 2023 M_w 7.8 and 7.7 events (USGS Geologic Hazards Science Center and Collaborators, 2023). Note that the scale bars are saturated at ±1 bar. The color version of this figure is available only in the electronic edition.

10 yr (until about 2030–2040; red–orange zones in Fig. 7c), and so aftershocks there were ongoing when the M_w 7.8 rupture struck.

Aftershocks of the M_w 7.8 mainshock are sparse or absent within the M_w 6.8 rupture zone, but are abundant beyond the rupture tips (see turquoise "M_w 6.8" labeled box in Fig. 5a). We calculate that the 2020 M_w 6.8 earthquake caused a 10-bar stress drop along the rupture, followed by the 1–2-bar stress increase imparted by the 2023 M_w 7.8 earthquake along the same section. So, the simplest explanation for why the high-slip zone of the 2020 shock is an aftershock "hole" in 2023 is that the stress decrease in 2020 was so much greater than the stress increase in 2023, and so 2023 M_w 7.8 aftershocks are inhibited there. This behavior can also be explained from a rate/state framework, in which a brief burst of aftershocks would be followed by an enduring aftershock hole, as found by Toda and Stein (2022), for megathrust earthquakes. This rate/state framework is presented in the forecast section.

Do Double Mainshocks Make Kahramanmaraş Aftershocks Unusually Productive?

Given the nature of the Kahramanmaraş sequence, one might expect its combined aftershock rate to be high, but instead it lands near the middle of its cohort (Fig. 8a). The number of $M_w \geq 4.5$ (or $M_w \geq 5.0$) Kahramanmaraş aftershocks resembles the 2016 M_w 7.8 Kaikōura earthquake, with the

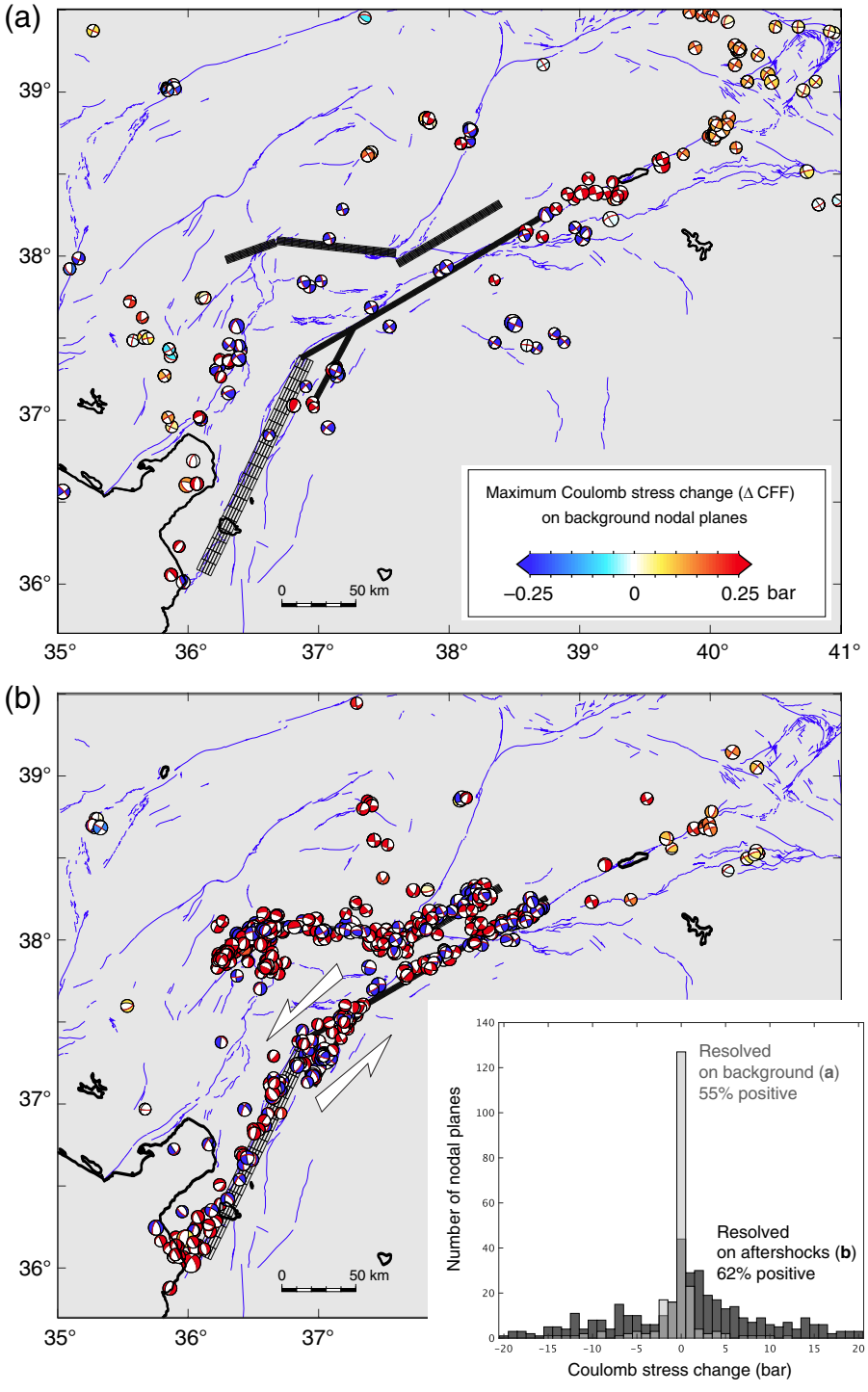

Figure 6. Coulomb stress change imparted by 2023 M_w 7.8 and 7.7 mainshocks resolved on focal mechanisms during the (a) background period and (b) aftershock period, with the scale bar saturated at ±0.25 bar so that remote stress changes are visible. Seismic station coverage was largely unchanged during these two periods. Here we plot the maximum Coulomb stress change; in other words, the stress change on the nodal plane most brought close to failure in each mechanism, with the selected plane marked by a thin red line when the figure is zoomed. Maximum Coulomb stress changes are thus "red biased," which is why, in the inset, the control percentage is 55% positive, rather than ~50%. Note the widespread presence of normal mechanisms, perhaps related to the southward 20° bend in the East Anatolian fault, similar to the northeast and southwest ends of the M_w 7.7 rupture zone. The color version of this figure is available only in the electronic edition.

2008 M_w 7.9 Wenchuan much higher, and the 2001 M_w 7.8 Kokoxili, Kunlun, and 2002 M_w 7.9 Denali shocks much lower. The slip rate of the East Anatolian (Emre *et al.*, 2018), Denali (Haeussler *et al.*, 2017), and Kunlun faults (Mohadjer *et al.*, 2017) are roughly comparable, at 5–13 mm/yr. Slip rates are lower on the Longmenshan fault (1.5 mm/yr, Wang *et al.*, 2008), on which the Wenchuan earthquake struck, and possibly also low on the many isolated segments of the Kaikōura rupture. This suggests that rougher or more low-slip-rate faults excite more aftershocks, perhaps because they lack a thick gouge layer, or contain more bends, breaks, and secondary faults, sites of aftershocks. There is also a weak correlation with seismic moment.

We can project the number of $M_w \geq 5.0$ shocks during the 12-month period beginning 1 December 2023 by fitting the data to an Omori decay (Fig. 8b), and then converting the $M_w \geq 4.5$ rate to $M_w \geq 5.0$ by assuming a *b*-value of 1.0. We expect 2.0 $M_w \geq 5.0$ shocks using the AFAD catalog, and 0.9 $M_w \geq 5.0$ shocks in the Advanced National Seismic System (ANSS) catalog. The decay rate slows beginning about a month after the mainshock in both AFAD and ANSS catalogs (Fig. 8b), and so these numbers might be underestimates.

Earthquake Forecast for the Next Twelve Months, 1 August 2023–31 July 2024

Our primary goal is to furnish a blind, testable forecast for a period short enough to enable

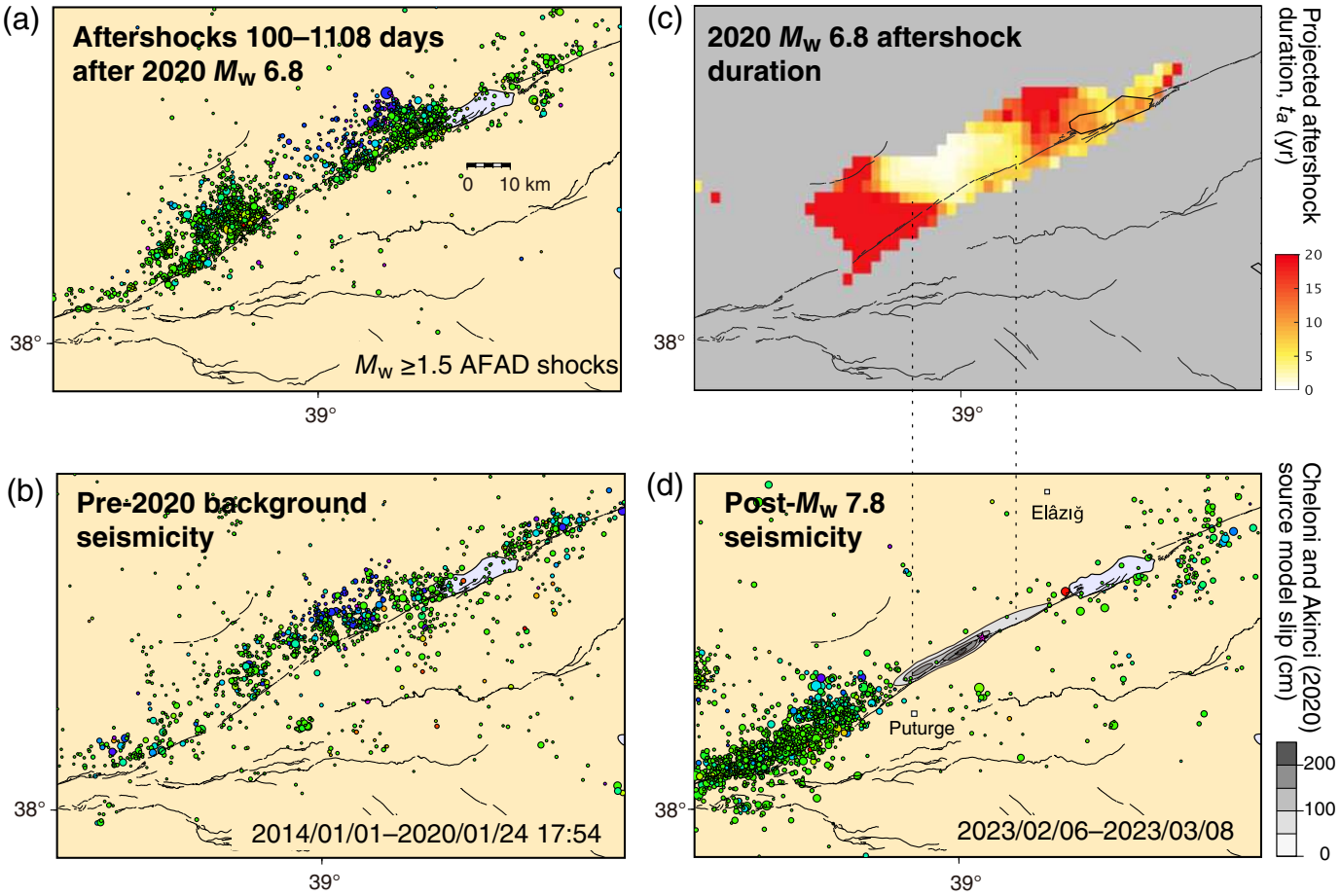

Figure 7. Seismicity after and before the 2020 M_w 6.8 and 2023 M_w 7.8 shocks. (a) Aftershocks are concentrated near the 2020 rupture tips, (b) unlike the more uniform background seismicity. We start 100 days after the mainshock when the magnitude of completeness drops to 1.5. (c) The aftershock duration is short in the high-slip zone, and long beyond it. (d) When the M_w 7.8 strikes, the M_w 6.8 high-slip area remains a seismicity hole for the 2023 aftershocks. There are also 2020 M_w 6.8 source models by Gallovič *et al.* (2020), Konca *et al.* (2021), and Taymaz *et al.* (2021); all show slip within 5–10 km of that by Cheloni and Akinci (2020). The color version of this figure is available only in the electronic edition.

us to learn from and improve future forecasts, here and elsewhere. If possible, we also seek to contribute to hazard mitigation and preparation in Eastern Türkiye.

The forecast is based on the modeled stress transfer, following Toda and Stein (2020). We calculate the Coulomb stress imparted to the nearest earthquake focal mechanisms (Fig. 6) assigned to $M_w \geq 2$ background earthquakes (magenta dots in Fig. 5a) as receivers. We use focal mechanisms rather than a uniform receiver fault strike, optimally oriented faults, or mapped faults. In Figures 1 and 2, we used mapped faults because those faults ruptured, and we have finite-fault models for their geometry and slip (Goldberg *et al.*, 2023). But for prospective forecasts, we find that focal mechanisms best capture the geometrical complexity of fault networks, and so provide more realistic results than the alternatives (Hardebeck *et al.*, 1998; Toda and Stein, 2020, 2022). Time dependence of the seismicity response to stress changes is incorporated though rate and state friction (Dieterich, 1994), in which stress changes amplify (if positive), or suppress (if negative) the background seismicity rate. Rate and state friction requires parameter assignments for two out of the three parameters: the expected aftershock duration (t_a), a constitutive parameter times the normal stress ($A\sigma$), and the stressing rate $\dot{\tau}$ (equation 19 in Dieterich, 1994). We set t_a to 5 yr based on the average projected aftershock decay of the 2020 M_w 6.8 events (Fig. 5c) as a representative value of the East Anatolian fault zone, and assign $A\sigma$ as 0.5 bar inferred from observations and widely applied (e.g., Toda *et al.*, 1998; Guatteri *et al.*, 2001; Catalli *et al.*, 2008). This results in a fault shear stressing rate $\dot{\tau}$ of 0.1 bar/yr, reasonable for the East Anatolian fault zone, with its 10 mm/yr slip rate.

After considering the AFAD, European-Mediterranean Seismological Centre, ANSS, and Global CMT catalogs, we used background seismicity r from the AFAD catalog, which is most complete. $M_c \geq 2$, but only since 2014 (Fig. S4). We ended the background period just before the 2020 M_w 6.8 shock, so its aftershocks would not be construed as background. The resulting observed ~5000 shocks are too sparse

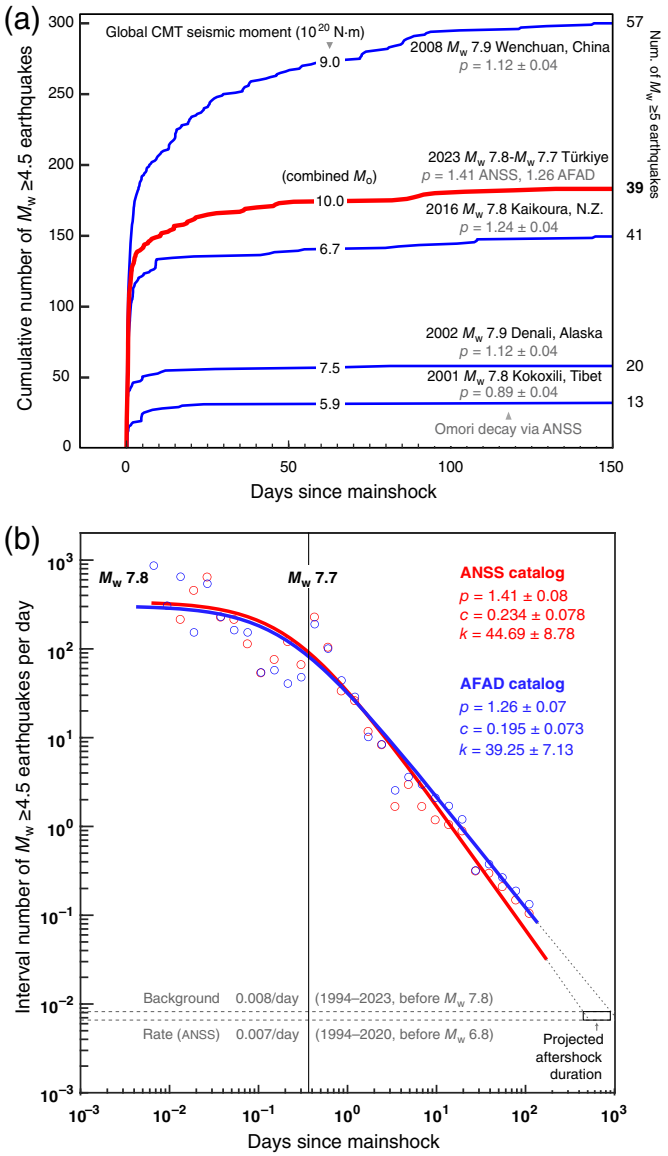

Figure 8. Kahramanmaraş aftershock decay compared with continental events of the same size. (a) 150-day aftershock productivity above the magnitude of completeness; aftershocks within 1° of the surface rupture are counted. The most productive mainshock struck on the fault with the lowest slip rate. There is a weak correlation of aftershock productivity with moment, but none with Omori decay. (b) Aftershock decay relative to the background seismicity rate. The aftershock duration lies at the intersection of the projected decay and the background rate. The color version of this figure is available only in the electronic edition.

to represent the spatial distribution of the background over the 400 × 525 km area, or one shock per 45 km^2. So, we instead used a smoothed, randomized background seismicity field keeping an overall rate equal to the 2014–2020 catalog. To reproduce the time-dependent seismicity perturbed by large earthquakes, we first compute steady-state variable γ_0 at each background earthquake from the following equation:

$$\gamma_0 = \frac{1}{\dot{\tau}}, \tag{1}$$

which is updated by subsequent earthquakes that brought Coulomb stress change ΔCFF on each assigned nodal plane (maximum ΔCFF chosen from two solutions) by the following equation:

$$\gamma_n = \gamma_{n-1} \exp\left(\frac{-\Delta\mathrm{CFF}}{A\sigma}\right), \tag{2}$$

in which the premainshock state variable γ_{n-1} changes to a new postmainshock value γ_n. The updated seismicity rate R at each background earthquake location in which r is set 1 initially (see fig. 9 in Toda and Stein, 2020) is then calculated from the following equation:

$$R = \frac{r}{\gamma\dot{\tau}}. \tag{3}$$

We used the five largest ($M_w \geq 6$) earthquakes since 2020 as sources, including the 2020 M_w 6.7 Doğanyol–Sivrice earthquake, 2023 M_w 7.8 Pazarcık earthquake, 2023 M_w 6.8 aftershock, 2023 M_w 7.7 Elbistan earthquake, and 2023 M_w 6.3 Antakya aftershock. We then convert the computed $M_w \geq 2$ rates into $M_w \geq 3$ rates for the retrospective test, and to $M_w \geq 5$ for prospective forecast, using $b = 0.86$ obtained from AFAD background catalog. Finally, to make the forecast maps (Fig. 9), we smoothed the calculated rates on randomized background epicenters using a 15-km radius moving cylinder on 0.06° × 0.06° grid nodes. We forecast the number of earthquakes retrospectively, adjusting the forecast by a multiplicative factor so that the total number of forecast earthquakes equals to the number observed (Fig. 9a). This forecast was then applied to the next 12 months starting from 1 December 2023 (Fig. 9b).

The retrospective forecast captures clusters of aftershocks along the ruptures and beyond their tips. Equally important, few if any aftershocks are seen in the stress shadows, which are the white lobes of very low or no forecast quakes. Nevertheless, there are two lobes of forecast seismicity empty of aftershocks, one between Elâzığ and Malatya, and the other southwest of Adiyaman (Fig. 9a). Whether these are inadequacies of the forecast, or sites of future shocks, remains to be seen.

The 12-month forecast reflects the rapidly decreasing frequency of aftershocks with time, and so the number of potentially damaging shocks expected in the next year is low. Nevertheless, we highlight 5–10 active faults (Emre *et al.*, 2018) near or in regions of higher-than-average earthquake rate (warm colors), as potential sites of $M_w \geq 5$ ruptures. In addition, some cities, already badly damaged in the Kahramanmaraş sequence, lie in regions of higher-than-average forecast aftershock activity, including Elâzığ, Malatya, and Antakya.

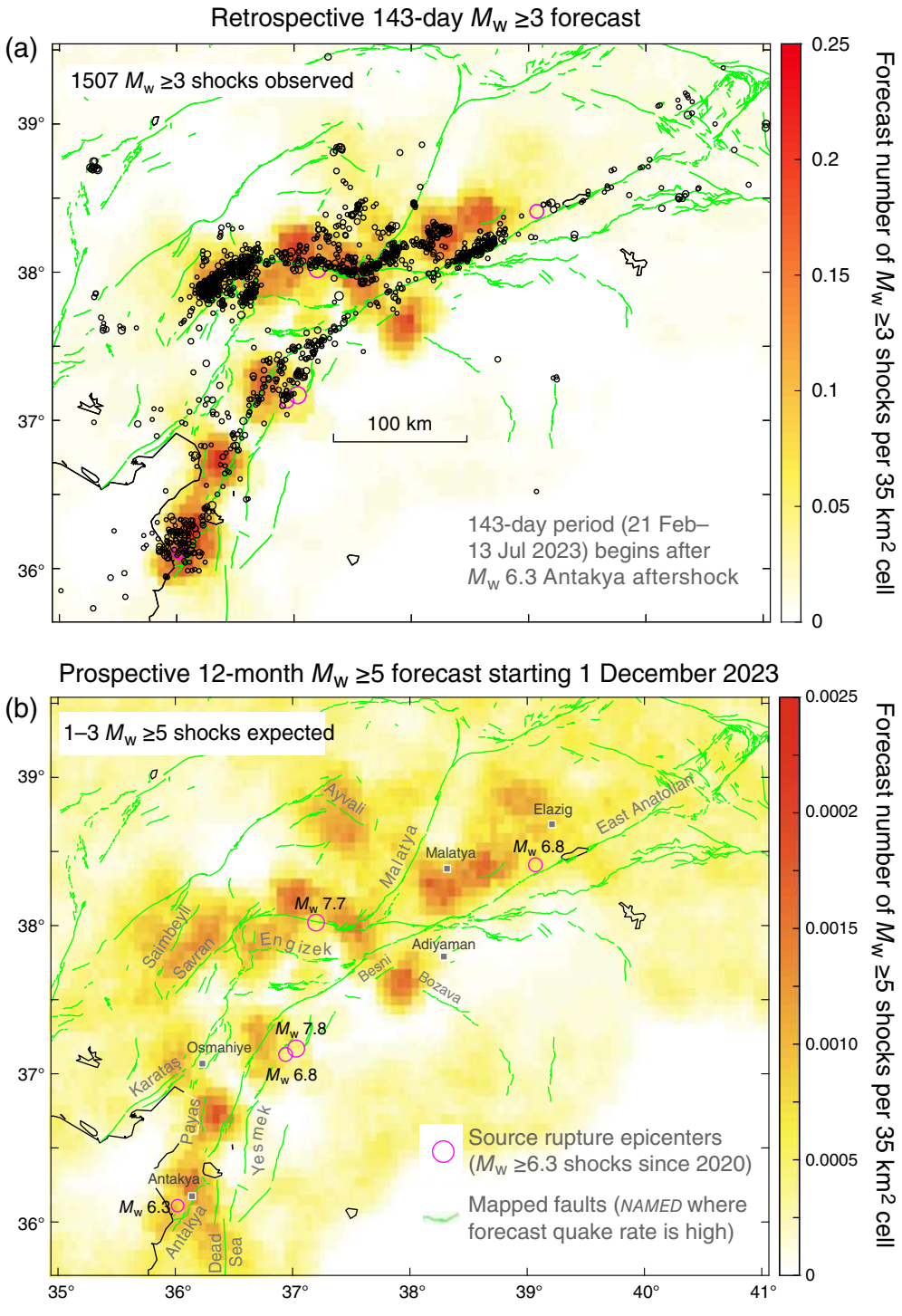

Figure 9. Kahramanmaraş regional forecasts. (a) The retrospective forecast captures the observed distribution of earthquakes well during the 143-day observation period, 21 February–13 July 2023. (b) We forecast 1–3 M_w ≥ 5 shocks during the period, 1 December 2023–30 November 2024. In both panels, stress shadows appear as white lobes, with lower quake rates than the background. Note that the color scale differs in each panel, and we caution that the forecast is unreliable in Syria due to inadequate seismic monitoring. The color version of this figure is available only in the electronic edition.

Conclusions

The three largest, closely spaced earthquakes are seen to toggle seismicity on and off. These effects are evident within hours of the mainshocks, in contrast to the view that dynamic triggering dominates in the first hours to days of a mainshock. We infer that the seismicity rate changes most likely result from the coseismic static stress changes. Nevertheless, the static shear stress drop along the eastern portion of the Çardak fault appears to have played no role in preventing that portion of the M_w 7.7 fault rupture. Thus, we infer that the large dynamic shear stress pulse in front of the moving rupture overwhelmed the much smaller static decrease, and so static stress changes appear to play little, if any, role in rupture propagation.

We argue not only that the M_w 7.8 shock promoted the second by about 3 bars, but that most of this occurred through unclamping of the M_w 7.7 epicentral patch, a phenomenon calculated for several other double events on relatively immature or slow slip-rate faults, as is the case for the Çardak fault.

For all three mainshocks, off-fault aftershocks generally occur in lobes where the stress is calculated to have increased, and tend to be sparse where the stress is calculated to have decreased. Two measures of the impact of Coulomb stress transfer to focal mechanisms, the increase in percentage of promoted mechanisms, and the mean stress change on aftershock versus background nodal planes, provide support for this inference. Three years after the 2020 M_w 6.8 Elâzığ shock, a seismicity rate drop in the central high-slip area persisted during the aftershock sequence of the M_w 7.8 shock. We speculate that fault sections that do not display aftershocks after large events, such as the high slip zone of the 2020 M_w 6.8 shock, may indicate the occurrence of recent,

historic, or paleoseismic shocks for which the cores remain shut down.

The 12-month earthquake forecast is intended to test the skill of our approach in understanding earthquake promotion and inhibition (Kagan and Jackson, 2011). Despite the relatively high Kahramanmaraş aftershock productivity, its rapid decay in the first 150 days suggests that the number of $M_w \geq 5$ shocks will, fortunately, be low. From this forecast, we hope to learn how such efforts can be improved. In the words of the late seismologist David D. Jackson (1943–2023), "Only prospective testing counts," and so herewith is our submission.

DATA AND RESOURCES

The U.S. Geological Survey (USGS) finite-fault source models for the 2023 M_w 7.8, 2023 M_w 7.7, and 2020 M_w 6.8 were accessed, respectively, from https://earthquake.usgs.gov/earthquakes/eventpage/us6000jllz/finite-fault, https://earthquake.usgs.gov/earthquakes/eventpage/us6000jlqa/finite-fault, and https://earthquake.usgs.gov/earthquakes/eventpage/us60007ewc/finite-fault for which their Coulomb input files are provided and downloadable. The authors used the Disaster and Emergency Management Authority of Türkiye (AFAD) hypocenter catalog, https://deprem.afad.gov.tr/event-catalog, and the AFAD focal mechanism catalog, https://deprem.afad.gov.tr/event-focal-mechanism. The authors used the active fault database of Emre *et al.* (2018), and Coulomb 3.4 (Toda *et al.*, 2005) for stress calculations, downloadable with a user guide at https://temblor.net/coulomb/. For magnitude of completeness calculations, we used ZMAP (Wiemer, 2001), available at http://www.seismo.ethz.ch/en/research-and-teaching/products-software/software/ZMAP/. All websites were last accessed in October 2023.

Declaration of Competing Interests

The authors acknowledge that there are declare no conflicts of interest recorded.

Acknowledgments

The authors thank Volkan Sevilgen, Ali Değer Özbakir, Hector Gonzales-Huizar, Myrto Papaspiliou, and Alexandra Tisoulu for perceptive comments and criticism. The authors gratefully acknowledge funding from the U.S. National Science Foundation (R. S. S.), the Willis Towers Watson Research Network (R. S. S. and S. T.), and the Oyo Corporation of Japan (S. T.).

References

Barnhart, W. D., G. P. Hayes, and R. D. Gold (2019). The July 2019 Ridgecrest, California, earthquake sequence: Kinematics of slip and stressing in cross-fault ruptures, *Geophys. Res. Lett.* **46,** 11,859–11,867, doi: 10.1029/2019GL084741.

Catalli, F., M. Cocco, R. Console, and L. Chiaraluce (2008). Modeling seismicity rate changes during the 1997 Umbria-Marche sequence (central Italy) though a rate- and state-dependent model, *J. Geophys. Res.* **113,** doi: 10.1029/2007JB005356.

Çetin, K. Ö, J. D. Bray, J. D. Frost, A. Hortacsu, E. Miranda, R. E. S. Moss, and J. P. Stewart (2023). 2023 Türkiye earthquakes: Report on geoscience and engineering impacts, *GEER Association Rept. 082*, Earthquake Engineering Research Institute, LFE Program, doi: 10.18118/G6PM34.

Cheloni, D., and A. Akinci (2020). Source modelling and strong ground motion simulations for the 24 January 2020, M_w 6.8 Elazığ earthquake, Turkey, *Geophys. J. Int.* **223,** 1054–1068, doi: 10.1093/gji/ggaa350.

Dieterich, J. H. (1994). A constitutive law for the rate of earthquake production and its application to earthquake clustering, *J. Geophys. Res.* **99,** 2601–2618, doi: 10.1029/93JB02581.

Duman, T.Y., and Ö. Emre (2013). The East Anatolian fault: Geometry, segmentation and jog characteristics, in *Geological Development of Anatolia and the Easternmost Mediterranean Region*, A. H. F. Robertson, O. Parlak, and U. C. Ünlügenç (Editors), Vol. 372, Geological Society, London, Special Publications, 495–529, doi: 10.1144/SP372.14.

Emre, Ö., T. Y. Duman, S. Özalp, F. Şaroğlu, Ş. Olgun, H. Elmacı, and T. Çan (2018). Active fault database of Turkey, *Bull. Earthq. Eng.* **16,** 3229–3275, doi: 10.1007/s10518-016-0041-2.

Erdik, M., M. B. D. Tümsa, A. Pınar, E. Altunel, and A. C. Zülfikar (2023). A preliminary report on the February 6, 2023 earthquakes in Türkiye, *Temblor*, doi: 10.32858/temblor.297.

Gallovič, F., J. Zahradník, V. Plicka, E. Sokos, C. Evangelidis, I. Fountoulakis, and F. Turhan (2020). Complex rupture dynamics on an immature fault during the 2020 M_w 6.8 Elazığ earthquake, Turkey, *Commun. Earth Environ.* **1,** 40, doi: 10.1038/s43247-020-00038-x.

Goldberg, D. E., T. Taymaz, N. G. Reitman, A. E. Hatem, S. Yolsal-Çevikbilen, W. D. Barnhart, T. S. Irmak, D. J. Wald, T. Öcalan, W. L. Yeck, *et al.* (2023). Rapid characterization of the February 2023 Kahramanmaraş, Türkiye, earthquake sequence, *The Seismic Record* **3,** 156–167, doi: 10.1785/0320230009.

Guatteri, M., P. Spudich, and G. C. Beroza (2001). Inferring rate and state friction parameters from a rupture model of the 1995 Hyogo-ken Nanbu (Kobe) Japan earthquake, *J. Geophys. Res.* **106,** 26,511–26,521, doi: 10.1029/2001JB000294.

Haeussler, P. J., A. Matmon, D. P. Schwartz, and G. G. Seitz (2017). Neotectonics of interior Alaska and the late Quaternary slip rate along the Denali fault system, *Geosphere* **13,** 1445–1463, doi: 10.1130/GES01447.1.

Hardebeck, J. L., J. J. Nazareth, and E. Hauksson (1998). The static stress change triggering model: Constraints from two southern California aftershock sequences, *J. Geophys. Res.* **103,** doi: 10.1029/98JB00573.

Hudnut, K. W., L. Seeber, and J. Pacheco (1989). Cross-fault triggering in the November 1987 Superstition Hills earthquake sequence, southern California, *Geophys. Res. Lett.* **16,** 199–202, doi: 10.1029/GL016i002p00199.

Hussain, E., S. Kalaycıoğlu, C. W. Milliner, and Z. Çakir (2023). Preconditioning the 2023 Kahramanmaraş (Türkiye) earthquake disaster, *Nat. Rev. Earth Environ.* **4,** 287–289, doi: 10.1038/s43017-023-00411-2.

Jia, Z., Z. Jin, M. Marchandon, T. Ulrich, A. A. Gabriel, W. Fan, P. Shearer, X. Zou, J. Rekoske, F. Bulut, *et al.* (2023). The complex dynamics of the 2023 Kahramanmaraş, Turkey, M_w 7.8-7.7 earthquake doublet, *Science* **381,** 985–990, doi: 10.1126/science.adi0685.

Kagan, Y. Y., and D. D. Jackson (2011). Global earthquake forecasts, *Geophys. J. Int.* **184,** 759–776, doi: 10.1111/j.1365-246X.2010.04857.x.

Karabacak, V., Ç. Özkaymak, H. Sözbilir, O. Tatar, B. Aktuğ, Ö. Cevdet Özdağ, R. Çakir, E. Aksoy, F. Koçbulut, M. Softa, *et al.* (2023). The 2023 Pazarcık (Kahramanmaraş, Türkiye) earthquake (M_w 7.7): Implications for surface rupture dynamics along the East Anatolian fault zone, *J. Geol. Soc.* **180,** doi: 10.1144/jgs2023-020.

Konca, A. Ö., H. Karabulut, S. E. Güvercin, F. Eskiköy, S. Özarpacı, A. Özdemir, M. Floyd, S. Ergintav, and U. Doğan (2021). From interseismic deformation with near-repeating earthquakes to co-seismic rupture: A unified view of the 2020 M_w 6.8 Sivrice (Elazığ) eastern Turkey earthquake, *J. Geophys. Res.* **126,** e2021JB021830 , doi: 10.1029/2021JB021830.

Melgar, D., T. Taymaz, A. Ganas, B. W. Crowell, T. Öcalan, M. Kahraman, V. Tsironi, S. Yolsal-Çevikbilen, S. Valkaniotis, T. S. Irmak, *et al.* (2023). Sub- and super-shear ruptures during the 2023 M_w 7.8 and 7.7 earthquake doublet in SE Türkiye, *Seismica*, doi: 10.26443/seismica.v2i3.387.

Mohadjer, S., T. A. Ehlers, R. Bendick, and S. G. Mutz (2017). Review of GPS and Quaternary fault slip rates in the Himalaya-Tibet orogen, *Earth Sci. Rev.* **174,** 39–52, doi: 10.1016/j.earscirev.2017.09.005.

Parsons, T. (2005). Significance of stress transfer in time-dependent earthquake probability calculations, *J. Geophys. Res.* **110,** no. B5, doi: 10.1029/2004JB003190.

Parsons, T., R. S. Stein, R. W. Simpson, and P. A. Reasenberg (1999). Stress sensitivity of fault seismicity: A comparison between limited-offset oblique and major strike-slip faults, *J. Geophys. Res.* **104,** 20,183–20,202, doi: 10.1029/1999JB900056.

Perfettini, H., R. S. Stein, R. Simpson, and M. Cocco (1999). Stress transfer by the 1988–1989 M = 5.3 and 5.4 Lake Elsman foreshocks to the Loma Prieta fault: Unclamping at the site of peak mainshock slip, *J. Geophys. Res.* **104,** 20,169–20,182, doi: 10.1029/1999JB900092.

Taymaz, T., A. Ganas, S. Yolsal-Çevikbilen, F. Vera, T. Eken, C. Erman, D. Keleş, V. Kapetanidis, S. Valkaniotis, I. Karasante, *et al.* (2021). Source mechanism and rupture process of the 24 January 2020 M_w 6.7 Doğanyol–Sivrice earthquake obtained from seismological waveform analysis and space geodetic observations on the East Anatolian fault zone (Turkey), *Tectonophysics* **804,** 228745, doi: 10.1016/j.tecto.2021.228745.

Toda, S., and R. S. Stein (2003). Toggling of seismicity by the 1997 Kagoshima earthquake couplet: A demonstration of time-dependent stress transfer, *J. Geophys. Res.* **108,** 2567 , doi: 10.1029/2003JB002527.

Toda, S., and R. S. Stein (2020). Long- and short-term stress interaction of the 2019 Ridgecrest sequence and Coulomb-based earthquake forecasts, *Bull. Seismol. Soc. Am.* **110,** 1765–1780, doi: 10.1785/0120200169.

Toda, S., and R. S. Stein (2022). Central shutdown and surrounding activation of aftershocks from megathrust earthquake stress transfer, *Nature Geosci.* **15,** 494–500, doi: 10.1038/s41561-022-00954-x.

Toda, S., R. S. Stein, A. D. Özbakir, H. Gonzalez-Huizar, V. Sevilgen, G. Lotto, and S. Sevilgen (2023). Stress change calculations provide clues to aftershocks in 2023 Türkiye earthquakes, *Temblor*, doi: 10.32858/temblor.295.

Toda, S., R. S. Stein, P. A. Reasenberg, J. H. Dieterich, and A. Yoshida (1998). Stress transferred by the M_w 6.5 Kobe, Japan, shock: Effect on aftershocks and future earthquake probabilities, *J. Geophys. Res.* **103,** 24,543–24,565, doi: 10.1029/98JB00765.

Toda, S., R. S. Stein, K. Richards-Dinger, and S. B. Bozkurt (2005). Forecasting the evolution of seismicity in southern California: Animations built on earthquake stress transfer, *J. Geophys. Res.* **110,** no. B5, doi: 10.1029/2004JB003415.

U.S. Geological Survey (USGS) Geologic Hazards Science Center and Collaborators (2023). The 2023 Kahramanmaraş, Turkey, Earthquake Sequence (as of February 22, 2023), available at https://earthquake.usgs.gov/storymap/index-turkey2023.html (last accessed July 2023).

Wang, Y., E. Wang, Z. Shen, M. Wang, W. Gan, X. Qiao, G. Meng, T. Li, W. Tao, Y. Yang, *et al.* (2008). GPS-constrained inversion of present-day slip rates along major faults of the Sichuan-Yunnan region, China, *Sci. China Earth Sci.* **51,** 1267–1283, doi: 10.1007/s11430-008-0106-4.

Wiemer, S. (2001). A software package to analyse seismicity: ZMAP, *Seismol. Res. Lett.* **72,** 373–382, doi: 10.1785/gssrl.72.3.373.

Manuscript received 28 July 2023
Published online 16 January 2024